Towards a Generic Radiative Transfer Model for the Earth's Surface-Atmosphere System: ESAS-Light

ESTEC Contract No AO/1-5433/07/NL/HE

# WP5100:

# Algorithm theoretical basis document for libRadtran (version 2.0-beta)

Arve Kylling, Claudia Emde, and Ulrich Hamann

Deutsches Zentrum für Luft- und Raumfahrt
Wessling, Germany

December 13, 2009

# Contents

# 1 Raman scattering

Air molecules scatter solar radiation. The effects of density, temperature, molecular (re)-orientation, and the role of kinetics, causing elastic and inelastic scattering, have primarily an effect on the spectral distribution of the scattered light. These phenomena splits the scattering into several components: (i) an elastic scattering component termed the Gross line, (ii) the Brillouin lines which describe inelastic translational Raman scattering and (iii) inelastic rotational and rotational-vibrational Raman scattering (Young, 1981b; Landgraf et al., 2004). In the Earth's atmosphere the Gross and Brillouin lines may be combined into one elastic scattering component, the so-called Cabannes line. To explain filling-in of Fraunhofer lines it suffices to account for Rayleigh scattering and rotational Raman scattering (Kattawar et al., 1981). The classical Rayleigh scattering cross section includes attenuation of energy due to wavelength redistribution by rotational Raman scattering (Young, 1981a). To account for Raman scattering the wavelength redistribution must be accounted for in the emitted energy.

Below a brief summary of Rayleigh and Raman scattering cross sections and phase functions is presented. The derivation of the one-dimensional radiative transfer equation including inelastic rotational Raman scattering may be found in for example Vountas et al. (1998) and will not be repeated here. Rather, the appropriate radiative transfer equation is presented and a discrete ordinate method solution outlined.

## 1.1 The Raman cross section and phase function

Molecular scattering of light in the Earth's atmosphere is caused by interactions of photons with $N_2$ and $O_2$ molecules and various trace gases. The effect of other gases than $N_2$ and $O_2$ on the filling-in of spectral lines and absorption lines is minor and will not be included in the discussion below. The cross section for rotational Raman scattering (RRS) by a linear molecule in units of $cm^2$ is (Chance and Spurr, 1997)

$$\sigma_{RRS}(\lambda_e,\lambda_s) = f_N(T)\gamma^2(\lambda_e)\frac{256\pi^5 C_{J\rightarrow J'}}{27\lambda_s^4}, \tag{1}$$

where $\lambda_e$ is the wavelength of the incoming radiation and $\lambda_s$ the wavelength of the scattered radiation. The wavelength shift is calculated from the energy difference between the initial and final state. It is taken from de Haan et al. (2003) together with the Placzek-Teller coefficients $C_{J\rightarrow J'}$.

The rotational angular quantum number is denoted by $N$ and $J$ and $J'$ are the total angular momentum for the inital and final states respectively. The total spin momentum quantum number $S$ is the difference between $J$ and $N$. For nitrogen $S = 0$ and for oxygen $S = 1$.

The polarizability anisotropy for $O_2$ and $N_2$ is (Chance and Spurr, 1997)

$$\gamma_{O_2}(\nu) = 7.149\times10^{-26}\mathrm{cm}^3 + \frac{4.59364\times10^{-15}\mathrm{cm}}{4.82716\times10^{9}\mathrm{cm}^{-2}-\nu^2} \tag{2}$$

$$\gamma_{N_2}(\nu) = -6.01466\times10^{-25}\mathrm{cm}^3 + \frac{2.38557\times10^{-14}\mathrm{cm}}{1.86099\times10^{10}\mathrm{cm}^{-2}-\nu^2} \tag{3}$$

where the wavenumber $\nu$ is in cm$^{-1}$.

The fraction $f_{N,J}(T)$ of molecules in the initial state at temperature $T$ is (Landgraf et al., 2004)

$$f_{N,J}(T) = \frac{g_N}{Z}(2J+1)\exp(-E_J/kT) \tag{4}$$

where $E_J$ is the rotational energy taken from de Haan et al. (2003).

The statistical weight factor $g_N$ for nitrogen is $g_N = 6$ and $g_N = 3$ for even and odd $J$, respectively. For oxygen, $g_N = 0$ and $g_N = 1$ for even and odd $J$, respectively. From the normalization condition

$$\sum f_{N,J} = 1, \tag{5}$$

the state sum $Z$ for pure rotational Raman scattering is determined.

The Raman phase function is given by (Landgraf et al., 2004; Spurr et al., 2008)

$$P^R(\Phi) = \frac{3}{40}(13+\cos^2\Phi) \tag{6}$$

and the corresponding Legendre expansion coefficient $g_2 = 1/20$.

## 1.2 The monochromatic radiative transfer equation

The one-dimensional equation for diffuse monochromatic radiation transport at wavelength $\lambda$ is given by (Chandrasekhar, 1950)

$$\begin{aligned}\mu\frac{dI(\tau_\lambda,\mu,\Phi)}{d\tau_\lambda} &= I(\tau_\lambda,\mu,\Phi) - \frac{\omega_\lambda(\tau_\lambda)}{4\pi}\int_0^{2\pi}d\Phi'\int_{-1}^{1}d\mu' P_\lambda(\tau_\lambda,\mu,\Phi;\mu',\Phi')I(\tau_\lambda,\mu',\Phi') \\ &\quad -\frac{\omega_\lambda(\tau_\lambda)I_\lambda^0}{4\pi}P_\lambda(\tau_\lambda,\mu,\Phi;-\mu_0,\Phi_0)e^{-T(\tau_\lambda)},\end{aligned} \tag{7}$$

where $I(\tau_\lambda,\mu,\Phi)$ is the radiance at optical depth $\tau_\lambda$ in direction $(\mu,\Phi)$, $\mu$ is the cosine of the polar angle and $\Phi$ is the azimuth angle. The solar beam direction is given by $(-\mu_0,\Phi_0)$. Furthermore, $\omega_\lambda(\tau_\lambda)$ is the single scattering albedo and $P_\lambda(\tau_\lambda,\mu,\Phi;\mu',\Phi')$ the phase function describing the likelihood of scattering from incident direction $(\mu',\Phi')$ into the direction $(\mu,\Phi)$. The incident flux is given by $\mu_0 I_\lambda^0$ and $e^{-T(\tau_\lambda)}$ is the beam transmittance for a slant optical thickness $T(\tau_\lambda)$. For the plane-parallel case $T(\tau_\lambda) = \tau_\lambda/\mu_0$. It is for this case that the DISORT (Stamnes et al., 1988) routine solves Eq. 7. For the pseudospherical case the transmittance is described by the Chapman function $ch$: $T(\tau_\lambda) = ch(\tau,\mu_0)$ (Dahlback and Stamnes, 1991). This version of Eq. 7 is solved by the sdisort solver which is part of the libRadtran software package (Mayer and Kylling, 2005).

## 1.3 The radiative transfer equation including Raman scattering

The radiative transfer equation including rotational Raman scattering has been derived by several authors (Landgraf et al., 2004; Vountas et al., 1998). Treating rotational Raman scattering as a first-order perturbation the radiative transfer equation becomes (Spurr et al., 2008)

$$\begin{aligned}\mu\frac{dI(\tau_\lambda,\mu,\Phi)}{d\tau_\lambda} &= I(\tau_\lambda,\mu,\Phi)-\frac{\omega_\lambda^C(\tau_\lambda)}{4\pi}\int_0^{2\pi}d\Phi'\int_{-1}^{1}d\mu' P_\lambda^C(\tau_\lambda,\mu,\Phi;\mu',\Phi')I(\tau_\lambda,\mu',\Phi')\\ &-\frac{\omega_\lambda^C(\tau_\lambda)I_\lambda^0}{4\pi}P_\lambda^C(\tau_\lambda,\mu,\Phi;-\mu_0',\Phi_0')e^{-T(\tau_\lambda)}\\ &-\sum_{s=1}^{NS}\frac{\omega_{\lambda_s}^R(\tau_{\lambda_s})}{4\pi}\int_0^{2\pi}d\Phi'\int_{-1}^{1}d\mu' P_{\lambda_s}^R(\tau_{\lambda_s},\mu,\Phi;\mu',\Phi')I(\tau_{\lambda_s},\mu',\Phi')\\ &-\sum_{s=1}^{NS}\frac{\omega_{\lambda_s}^R(\tau_{\lambda_s})I_{\lambda_s}^0}{4\pi}P_{\lambda_s}^R(\tau_{\lambda_s},\mu,\Phi;-\mu_0',\Phi_0')e^{-T(\tau_{\lambda_s})}. \qquad (8)\end{aligned}$$

Here the single scattering albedo for elastic scattering and the corresponding phase function is denoted by $\omega_\lambda^C(\tau_\lambda)$ and $P_\lambda^C(\tau_\lambda,\mu,\Phi;\mu',\Phi')$, respectively, and is the contribution from molecular Cabannes scattering. The Raman gain single scattering albedo is $\omega_{\lambda_s}^R(\tau_{\lambda_s})$ and the Raman phase function $P_{\lambda_s}^R(\tau_{\lambda_s},\mu,\Phi;\mu',\Phi')$, while $\tau_{\lambda_s}$ is the optical depth at the Raman shifted wavelength $\lambda_s$. The two last terms in Eq. 8 represents Raman inelastically scattered light from Raman-shifted wavelengths.

Using the following relationship

$$\omega_\lambda^E(\tau_\lambda)P_\lambda^E(\tau_\lambda,\mu,\Phi;-\mu',\Phi')=\omega_\lambda^C(\tau_\lambda)P_\lambda^C(\tau_\lambda,\mu,\Phi;-\mu',\Phi')+\omega_\lambda^{RL}(\tau_\lambda)P_\lambda^{RL}(\tau_\lambda,\mu,\Phi;-\mu',\Phi') \qquad (9)$$

Eq. 8 may be rewritten according to Spurr et al. (2008) as:

$$\begin{aligned}\mu\frac{dI(\tau_\lambda,\mu,\Phi)}{d\tau_\lambda} &= I(\tau_\lambda,\mu,\Phi)-\frac{\omega_\lambda^E(\tau_\lambda)}{4\pi}\int_0^{2\pi}d\Phi'\int_{-1}^{1}d\mu' P_\lambda^E(\tau_\lambda,\mu,\Phi;\mu',\Phi')I(\tau_\lambda,\mu',\Phi')\\ &-\frac{\omega_\lambda^E(\tau_\lambda)I_\lambda^0}{4\pi}P_\lambda^E(\tau_\lambda,\mu,\Phi;-\mu_0',\Phi_0')e^{-T(\tau_\lambda)}\\ &+\frac{\omega_\lambda^{RL}(\tau_\lambda)}{4\pi}\int_0^{2\pi}d\Phi'\int_{-1}^{1}d\mu' P_\lambda^R(\tau_\lambda,\mu,\Phi;\mu',\Phi')I(\tau_\lambda,\mu',\Phi')\\ &+\frac{\omega_\lambda^{RL}(\tau_\lambda)I_\lambda^0}{4\pi}P_\lambda^R(\tau_\lambda,\mu,\Phi;-\mu_0',\Phi_0')e^{-T(\tau_\lambda)}\\ &-\sum_{s=1}^{NS}\frac{\omega_{\lambda_s}^R(\tau_{\lambda_s})}{4\pi}\int_0^{2\pi}d\Phi'\int_{-1}^{1}d\mu' P_{\lambda_s}^R(\tau_{\lambda_s},\mu,\Phi;\mu',\Phi')I(\tau_{\lambda_s},\mu',\Phi')\\ &-\sum_{s=1}^{NS}\frac{\omega_{\lambda_s}^R(\tau_{\lambda_s})I_{\lambda_s}^0}{4\pi}P_{\lambda_s}^R(\tau_{\lambda_s},\mu,\Phi;-\mu_0',\Phi_0')e^{-T(\tau_{\lambda_s})}. \qquad (10)\end{aligned}$$

### 1.3.1 The radiative transfer equation for first-order Raman scattering

In the first-order Raman scattering approximation the undisturbed zeroth order or elastic scattering only, Eq. 7, is solved first. This gives the elastic radiance $I^E(\tau_\lambda,\mu,\Phi)$ which is inserted into the 4th and 6th terms on the right side of Eq. 10 to yield:

$$\begin{aligned}
\mu\frac{dI(\tau_\lambda,\mu,\Phi)}{d\tau_\lambda} &= I(\tau_\lambda,\mu,\Phi)-\frac{\omega_\lambda^E(\tau_\lambda)}{4\pi}\int_0^{2\pi}d\Phi'\int_{-1}^{1}d\mu' P_\lambda^E(\tau_\lambda,\mu,\Phi;\mu',\Phi')I(\tau_\lambda,\mu',\Phi') \\
&\quad -\frac{\omega_\lambda^E(\tau_\lambda)I_\lambda^0}{4\pi}P_\lambda^E(\tau_\lambda,\mu,\Phi;-\mu_0',\Phi_0')e^{-T(\tau_\lambda)} \\
&\quad +\frac{\omega_\lambda^{RL}(\tau_\lambda)}{4\pi}\int_0^{2\pi}d\Phi'\int_{-1}^{1}d\mu' P_\lambda^R(\tau_\lambda,\mu,\Phi;\mu',\Phi')I^E(\tau_\lambda,\mu',\Phi') \\
&\quad +\frac{\omega_\lambda^{RL}(\tau_\lambda)I_\lambda^0}{4\pi}P_\lambda^R(\tau_\lambda,\mu,\Phi;-\mu_0',\Phi_0')e^{-T(\tau_\lambda)} \\
&\quad -\sum_{s=1}^{NS}\frac{\omega_{\lambda_s}^R(\tau_{\lambda_s})}{4\pi}\int_0^{2\pi}d\Phi'\int_{-1}^{1}d\mu' P_{\lambda_s}^R(\tau_{\lambda_s},\mu,\Phi;\mu',\Phi')I^E(\tau_{\lambda_s},\mu',\Phi') \\
&\quad -\sum_{s=1}^{NS}\frac{\omega_{\lambda_s}^R(\tau_{\lambda_s})I_{\lambda_s}^0}{4\pi}P_{\lambda_s}^R(\tau_{\lambda_s},\mu,\Phi;-\mu_0',\Phi_0')e^{-T(\tau_{\lambda_s})}. \qquad (11)
\end{aligned}$$

Eq. 11 may be rewritten

$$\begin{aligned}
\mu\frac{dI(\tau_\lambda,\mu,\Phi)}{d\tau_\lambda} &= I(\tau_\lambda,\mu,\Phi)-\frac{\omega_\lambda^E(\tau_\lambda)}{4\pi}\int_0^{2\pi}d\Phi'\int_{-1}^{1}d\mu' P_\lambda^E(\tau_\lambda,\mu,\Phi;\mu',\Phi')I(\tau_\lambda,\mu',\Phi') \\
&\quad -\frac{\omega_\lambda^E(\tau_\lambda)I_\lambda^0}{4\pi}P_\lambda^E(\tau_\lambda,\mu,\Phi;-\mu_0',\Phi_0')e^{-T(\tau_\lambda)} \\
&\quad -Q(\tau_\lambda,\mu,\Phi), \qquad (12)
\end{aligned}$$

where the source term

$$\begin{aligned}
Q(\tau_\lambda,\mu,\Phi) &= +\sum_{s=1}^{NS}\frac{\omega_{\lambda_s}^R(\tau_{\lambda_s})}{4\pi}\int_0^{2\pi}d\Phi'\int_{-1}^{1}d\mu' P_{\lambda_s}^R(\tau_{\lambda_s},\mu,\Phi;\mu',\Phi')I^E(\tau_{\lambda_s},\mu',\Phi') \\
&\quad +\sum_{s=1}^{NS}\frac{\omega_{\lambda_s}^R(\tau_{\lambda_s})I_{\lambda_s}^0}{4\pi}P_{\lambda_s}^R(\tau_{\lambda_s},\mu,\Phi;-\mu_0',\Phi_0')e^{-T(\tau_{\lambda_s})} \\
&\quad -\frac{\omega_\lambda^{RL}(\tau_\lambda)}{4\pi}\int_0^{2\pi}d\Phi'\int_{-1}^{1}d\mu' P_\lambda^R(\tau_\lambda,\mu,\Phi;\mu',\Phi')I^E(\tau_\lambda,\mu',\Phi') \\
&\quad -\frac{\omega_\lambda^{RL}(\tau_\lambda)I_\lambda^0}{4\pi}P_\lambda^R(\tau_\lambda,\mu,\Phi;-\mu_0',\Phi_0')e^{-T(\tau_\lambda)}. \qquad (13)
\end{aligned}$$

### 1.3.2 A discrete ordinate method solution

In the discrete ordinate method the azimuth dependence is separated by expanding the radiance as a Fourier cosine series (Chandrasekhar, 1950, p. 149-150):

$$I(\tau_\lambda,\mu,\Phi)=\sum_{m=0}^{2M-1} I(\tau_\lambda,\pm\mu)\cos m(\Phi_0-\Phi). \tag{14}$$

Furthermore the phase function is written in terms of Legendre polynomials $P_l(\cos\Theta)$:

$$P(\tau,\mu,\Phi;\mu',\Phi')=P(\tau,\cos\Theta)=\sum_{l=0}^{2M-1}(2l+1)g_l(\tau)P_l(\cos\Theta), \tag{15}$$

where the expansion coefficients are given by

$$g_l(\tau)=\frac{1}{2}\int_{-1}^{1}P_l(\cos\Theta)P(\tau,\cos\Theta)d\cos\Theta. \tag{16}$$

Using the relation

$$\cos\Theta=-\mu'\mu+\sqrt{1-\mu'^2}\sqrt{1-\mu^2}\cos(\Phi-\Phi'), \tag{17}$$

and applying the addition theorem for spherical harmonics (see Jackson (1975, p. 100-102) for a proof of the addition theorem for spherical harmonics) to Eq. 15 the following expression is obtained for the phase function:

$$\begin{aligned}
P(\tau,\mu,\Phi;\mu',\Phi') &= P(\tau,\cos\Theta)\\
&= \sum_{l=0}^{2M-1}(2l+1)g_l(\tau)\Big\{P_l(\mu)P_l(\mu')+2\sum_{m=1}^{l}\Lambda_l^m(\mu)\Lambda_l^m(\mu')\cos m(\phi-\phi')\Big\}\\
&= \sum_{m=0}^{2M-1}(2-\delta_{0,m})\Big\{\sum_{l=m}^{2M-1}(2l+1)g_l(\tau)\Lambda_l^m(\mu)\Lambda_l^m(\mu')\Big\}\cos m(\phi-\phi')
\end{aligned} \tag{18}$$

where the order of summation has been changed between the two last lines and $\Lambda_l^m(\mu)$ is the normalized associated Legendre polynomial which are preferred instead of the associated Legendre polynomials for numerical reasons (Stamnes et al., 2000, section 3.3.2).

Insertion of Eqs. 14 and 18 into Eq. 12 and performing the integrals over $\Phi'$ gives for each Fourier component the following equation:

$$\begin{aligned}
\mu\frac{dI^m(\tau_\lambda,\mu)}{d\tau_\lambda} &= I^m(\tau_\lambda,\mu)-\frac{\omega_\lambda^E(\tau_\lambda)}{2}\int_{-1}^{1}d\mu'\Pi_d^{E,m}(\tau_{\lambda_s},\mu,\mu')I^m(\tau_\lambda,\mu')\\
&\quad -\frac{\omega_\lambda^E(\tau_\lambda)I_\lambda^0}{4\pi}(2-\delta_{0,m})\Pi_b^{E,m}(\tau_\lambda,\mu,-\mu_0)e^{-T(\tau_\lambda)}\\
&\quad -Q^m(\tau_\lambda,\mu),
\end{aligned} \tag{19}$$

where the source term

$$
\begin{aligned}
Q^m(\tau_\lambda,\mu) = \quad & +\sum_{s=1}^{NS}\frac{\omega_{\lambda_s}^R(\tau_{\lambda_s})}{2}\int_{-1}^{1}d\mu'\Pi_d^{R,m}(\tau_{\lambda_s},\mu,\mu')I^{E,m}(\tau_{\lambda_s},\mu') \\
& +\sum_{s=1}^{NS}\frac{\omega_{\lambda_s}^R(\tau_{\lambda_s})I_{\lambda_s}^0}{4\pi}(2-\delta_{0,m})\Pi_b^{R,m}(\tau_{\lambda_s},\mu,\mu_0)e^{-T(\tau_{\lambda_s})} \\
& -\frac{\omega_\lambda^{RL}(\tau_\lambda)}{2}\int_{-1}^{1}d\mu'\Pi_d^{R,m}(\tau_\lambda,\mu,\mu')I^{E,m}(\tau_\lambda,\mu') \\
& -\frac{\omega_\lambda^{RL}(\tau_\lambda)I_\lambda^0}{4\pi}(2-\delta_{0,m})\Pi_b^{R,m}(\tau_\lambda,\mu,\mu_0)e^{-T(\tau_\lambda)}. \qquad (20)
\end{aligned}
$$

and

$$
\begin{aligned}
\Pi_b^{x,m}(\tau,\mu,\mu') &= \sum_{l=m}^{2M-1}(2l+1)g_l^x(\tau)(-1)^{l+m}\Lambda_l^m(\mu)\Lambda_l^m(\mu_0) \qquad (21)\\
\Pi_d^{x,m}(\tau,\mu,\mu') &= \sum_{l=m}^{2M-1}(2l+1)g_l^x(\tau_{\lambda_s})\Lambda_l^m(\mu)\Lambda_l^m(\mu'), \qquad (22)
\end{aligned}
$$

where $x = E,R$. It is noted that for $x = R$ only terms for $m = 0,1,2$ contribute in the above sums, see Raman phase function Eq. 6. For Raman scattering the different terms become:

$$
\begin{aligned}
m=0, l=0 &: \Lambda_0^0(\mu)\Lambda_0^0(\mu_0) \qquad (23)\\
m=0, l=2 &: 5g_2^R\Lambda_2^0(\mu)\Lambda_2^0(\mu_0) \qquad (24)\\
m=1, l=2 &: -5g_2^R\Lambda_2^1(\mu)\Lambda_2^1(\mu_0) \qquad (25)\\
m=2, l=2 &: 5g_2^R\Lambda_2^2(\mu)\Lambda_2^2(\mu_0). \qquad (26)
\end{aligned}
$$

By replacing the integrals in Eq. 19 with a sum using double Gaussian quadrature the discrete

ordinate solution of Eq. 19 is obtained (Chandrasekhar, 1950; Stamnes et al., 1988):

$$\begin{aligned}
\mu_i \frac{dI^m(\tau_\lambda,\mu_i)}{d\tau_\lambda} &= I^m(\tau_\lambda,\mu_i) - \frac{\omega^E_\lambda(\tau_\lambda)}{2}\sum_{\substack{j=-1\\ j\neq 0}}^{j=1} c_j \Pi^E_d(\tau_{\lambda_s},\mu_i,\mu_j) I^m(\tau_\lambda,\mu_j) \\
&\quad - \frac{\omega^E_\lambda(\tau_\lambda) I^0_\lambda}{4\pi}(2-\delta_{0,m})\Pi^E_b(\tau_{\lambda_s},\mu_i,\mu_0) e^{-T(\tau_\lambda)} \\
&\quad - Q^m(\tau_\lambda,\mu_i), \qquad (27)\\
Q^m(\tau_\lambda,\mu_i) = &\quad + \sum_{s=1}^{NS}\frac{\omega^R_{\lambda_s}(\tau_{\lambda_s})}{2}\sum_{\substack{j=-1\\ j\neq 0}}^{j=1} c_j \Pi^R_d(\tau_{\lambda_s},\mu_i,\mu_j) I^{E,m}(\tau_{\lambda_s},\mu_j) \\
&\quad + \sum_{s=1}^{NS}\frac{\omega^R_{\lambda_s}(\tau_{\lambda_s}) I^0_{\lambda_s}}{4\pi}(2-\delta_{0,m})\Pi^R_b(\tau_{\lambda_s},\mu_i,\mu_0) e^{-T(\tau_{\lambda_s})} \\
&\quad - \frac{\omega^{RL}_\lambda(\tau_\lambda)}{2}\sum_{\substack{j=-1\\ j\neq 0}}^{j=1} c_j \Pi^R_d(\tau_\lambda,\mu_i,\mu_j) I^{E,m}(\tau_\lambda,\mu_j) \\
&\quad - \frac{\omega^{RL}_\lambda(\tau_\lambda) I^0_\lambda}{4\pi}(2-\delta_{0,m})\Pi^R_b(\tau_\lambda,\mu_i,\mu_0) e^{-T(\tau_\lambda)}, \qquad (28)
\end{aligned}$$

where $\mu_i$ and $c_i$ are quadrature angles and weights respectively.

Eqs. 27-28 are a system of $2N$ coupled differential equations for which analytic solutions do not exist. A solution of an equation similar to Eq. 27, but with a general source term instead of direct beam source term and the Raman scattering source terms, has been given by Kylling and Stamnes (1992). The qdisort solver included in libRadtran, is an implementation of this solution procedure. In addition to the particular solution for the general source term it also includes particular solutions for the direct beam source and optionally a thermal source. The solution of the transport equation for a general source term is given in Kylling and Stamnes (1992) and will not be repeated here.

The three different single scattering albedos for the elastic, Raman gain and Raman loss scattering terms, are calculated according to Stamnes (1986); Spurr et al. (2008) as:

$$\omega^E_\lambda(\tau_\lambda) = \frac{\beta^{\text{sca}}(z,\lambda)}{\beta^{\text{ext}}(z,\lambda)} \qquad (29)$$

$$\omega^R_\lambda(\tau_{\lambda_s}) = \frac{\rho_{\text{air}}(z)(\zeta_{\text{O}_2}\sigma_{RRS,\text{O}_2}(\lambda_s,\lambda)+\zeta_{\text{N}_2}\sigma_{RRS,\text{N}_2}(\lambda_s,\lambda))}{\beta^{\text{ext}}(z,\lambda)} \qquad (30)$$

$$\omega^{RL}_\lambda(\tau_\lambda) = \frac{\rho_{\text{air}}(z)(\zeta_{\text{O}_2}\sum_{s=1}^{NS\_\text{O}_2}\sigma_{RRS,\text{O}_2}(\lambda,\lambda_s)+\zeta_{\text{N}_2}\sum_{s=1}^{NS\_\text{N}_2}\sigma_{RRS,\text{N}_2}(\lambda,\lambda_s))}{\beta^{\text{ext}}(z,\lambda)} \qquad (31)$$

where

$$\beta^{\text{sca}}(z,\lambda) = \sum_i \beta^{\text{sca}}_i(z,\lambda), \qquad \beta^{\text{sca}}_i(z,\lambda) = n_i(z)\sigma^{\text{sca}}_i(z,\lambda) \qquad (32)$$

$$\beta^{\text{abs}}(z,\lambda) = \sum_i \beta^{\text{abs}}_i(z,\lambda), \qquad \beta^{\text{abs}}_i(z,\lambda) = n_i(z)\sigma^{\text{abs}}_i(z,\lambda) \qquad (33)$$

and

$$\beta^{\text{ext}}(z,\lambda) = \beta^{\text{abs}}(z,\lambda) + \beta^{\text{sca}}(z,\lambda). \tag{34}$$

Furthermore, the relative abundance of $O_2$ and $N_2$ are set to $\zeta_{O_2} = 0.2095$ and $\zeta_{N_2} = 0.7905$. The elastic single scattering albedo $\omega_\lambda^E$ is the same as used in the elastic calculation.

# 2 3D polarized radiative transfer

Observations of polarized radiance may provide much more detailed information about atmospheric constituents than unpolarized measurements, in particular about aerosol and cloud optical and microphysical properties. However, polarization of atmospheric radiation is neglected by most radiative transfer models, although even the error in the unpolarized radiance may amount to 10%.

## 2.1 Monte Carlo Method for polarized radiative transfer

The Monte Carlo solver MYSTIC (Mayer, 2000; Emde and Mayer, 2007) has been extended to solve the vector radiative transfer equation.

Additions to a scalar Monte Carlo model that are required to implement polarization by Rayleigh, aerosol, and cloud scattering are described in Emde et al. (2009). The following algorithm description is mostly from this publication.

To implement polarization, one possibility is to assign a random polarization state to each traced photon entering the atmosphere. Another more efficient possibility is to interpret each traced photon as a photon package and to assign a weight vector corresponding to the Stokes parameters to each package. The following example demonstrates why the weight vector method is more efficient: Circular polarization is not influenced by the atmosphere, so the average of the circular component of the polarization state is zero before the photons enter the atmosphere and it will still be negligible when the photons are measured at the surface. The contributions by left and right circular polarized photons to the total circular polarisation cancel each other. In the weight vector method all photon packages contribute to the result, therefore we have implemented this method.

The Stokes parameters are defined as time averages of linear combinations of the electromagnetic field vector (Chandrasekhar, 1950; Hansen and Travis, 1974; Mishchenko et al., 2002):

$$I = \langle E_l E_l^* + E_r E_r^* \rangle , \tag{35}$$

$$Q = \langle E_l E_l^* - E_r E_r^* \rangle , \tag{36}$$

$$U = \langle E_l E_r^* + E_r E_l^* \rangle , \tag{37}$$

$$V = i \langle E_l E_r^* - E_r E_l^* \rangle . \tag{38}$$

Here, $E_l$ and $E_r$ are the components of the electric field vector parall**e**l and perpendicula**r** to the reference plane respectively. The model coordinate system is defined by the vertical (z-axis), the Southern direction (x-axis) and the Eastern direction (y-axis). The Stokes vector is defined in the reference frame defined by the z-axis and the propagation direction of the radiation. Since the Stokes parameters are real-valued and have the dimension of intensity, they can be measured directly with suitable instruments. The Stokes parameters define a complete set of quantities needed to characterize a plane electromagnetic wave as they carry information of the complex amplitudes and the phase difference.

The initial Stokes weight vector for solar radiation is $\mathbf{I}_w^0 = (1,0,0,0)$ corresponding to the unpolarized extraterrestrial solar radiation. The initial direction of the photon is defined by the

solar zenith angle and the solar azimuth angle.

For randomly oriented particles absorption does not depend on the polarization state of the radiation. In MYSTIC absorption is considered by reducing the photon weight $w_a$ according to Lambert-Beer's Law :

$$w_a = \exp\left(-\int \beta_{\text{abs}} \mathrm{d}s\right). \tag{39}$$

Here d$s$ is a path element of the photon path and $\beta_{\text{abs}}$ is the total absorption coefficient including molecules, aerosols, and water and ice clouds.

The free path of a photon until a scattering interaction takes place is sampled according to the probability density function (PDF)

$$P_s = \exp\left(-\int_0^s \beta_{\text{sca}} \mathrm{d}s'\right). \tag{40}$$

Here, $\beta_{\text{sca}} = \sum_{i=1}^{N} \beta_{\text{sca,i}}$ is the total scattering coefficient of $N$ interacting particles and molecules. This formula is valid for randomly oriented particles (i.e. with diagonal extinction matrix).

We use a random number $r \in [0,1]$ to decide which interaction takes place. If there are $N$ types of particles and molecules at the place of scattering, the photon interacts with the $j^{th}$ type if the random number fulfills the following condition:

$$\frac{\sum_{i=1}^{j-1} \beta_{\text{sca,i}}}{\beta_{\text{sca}}} < r \leq \frac{\sum_{i=1}^{j} \beta_{\text{sca,i}}}{\beta_{\text{sca}}}. \tag{41}$$

The next step is to sample the new photon direction. For scalar radiative transfer and randomly oriented particles the scattering direction depends only on the scattering zenith angle, not on the azimuth. Then the scattering phase function is used as the PDF to sample the new direction.

For polarized radiative transfer the scattering interaction is described by the scattering phase matrix. For convenience the scattering phase matrix is defined in the scattering frame, i.e. the coordinate system defined by the plane of the incoming $\mathbf{n}^{\text{inc}}$ and the scattered $\mathbf{n}^{\text{sca}}$ photon directions and a vector orthogonal to this plane (see Fig. 1), where the phase matrix depends only on the scattering angle $\Theta$. For randomly oriented particles, six matrix elements are required (van de Hulst, 1981):

$$\mathbf{P}(\Theta) = \begin{bmatrix} P_{11}(\Theta) & P_{12}(\Theta) & 0 & 0 \\ P_{12}(\Theta) & P_{22}(\Theta) & 0 & 0 \\ 0 & 0 & P_{33}(\Theta) & P_{34}(\Theta) \\ 0 & 0 & -P_{34}(\Theta) & P_{44}(\Theta) \end{bmatrix}, \tag{42}$$

while for spherical particles only four elements are required because $P_{11} = P_{22}$ and $P_{33} = P_{44}$. The Stokes weight vector is defined in the reference coordinate system in the plane given by the propagation direction of the radiation and the $z$-axis. Hence, to apply the phase matrix to the Stokes weight vector one has to rotate the Stokes weight vector into the scattering frame. After multiplication with the phase matrix it is rotated back to the reference coordinate system:

$$\mathbf{I}^{\text{sca}} = \mathbf{L}(\sigma_2)\mathbf{P}\mathbf{L}(\sigma_1)\mathbf{I}^{\text{inc}} = \mathbf{Z}\mathbf{I}^{\text{inc}}, \tag{43}$$

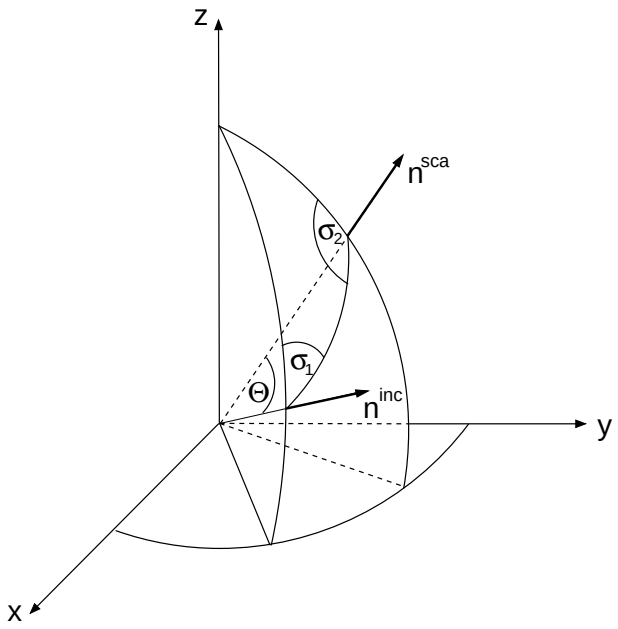


Figure 1: Incoming $\mathbf{n}^{\text{inc}}$ and scattered $\mathbf{n}^{\text{sca}}$ directions in the model coordinate system (x,y,z). $\sigma_1$ and $\sigma_2$ are the rotation angles to transform the Stokes vector from the reference frame to the scattering frame and vice versa and $\Theta$ is the scattering angle. The scattering plane is defined by the vectors $\mathbf{n}^{\text{inc}}$ and $\mathbf{n}^{\text{sca}}$. Figure adapted from Mishchenko et al. (2002).

where $\mathbf{I}^{\text{inc}}$ and $\mathbf{I}^{\text{sca}}$ are the incoming and scattered Stokes vectors respectively, $\sigma_1$ and $\sigma_2$ are the rotation angles for the Stokes vector, $\mathbf{Z}$ is the scattering matrix and $\mathbf{L}(\alpha)$ is the Stokes rotation matrix:

$$\mathbf{L}(\alpha) = \begin{bmatrix} 1 & 0 & 0 & 0 \\ 0 & \cos(2\alpha) & -\sin(2\alpha) & 0 \\ 0 & \sin(2\alpha) & \cos(2\alpha) & 0 \\ 0 & 0 & 0 & 1 \end{bmatrix}. \tag{44}$$

The rotation angles $\sigma_1$ and $\sigma_2$ are calculated from the incoming $\mathbf{n}^{\text{inc}}(\theta^{\text{inc}}, \phi^{\text{inc}})$ and the scattered $\mathbf{n}^{\text{sca}}(\theta^{\text{sca}}, \phi^{\text{sca}})$ directions as follows:

$$\sigma_1 = \arccos((\mathbf{n}^{\text{inc}} \times \mathbf{n}^{\text{z}}) \cdot (\mathbf{n}^{\text{inc}} \times \mathbf{n}^{\text{sca}})), \tag{45}$$

$$\sigma_2 = \arccos((\mathbf{n}^{\text{sca}} \times \mathbf{n}^{\text{z}}) \cdot (\mathbf{n}^{\text{sca}} \times \mathbf{n}^{\text{inc}})). \tag{46}$$

Here, $\mathbf{n}^{\text{z}}$ is the unit vector in $z$-direction (0,0,1).

The scattering matrix $\mathbf{Z}$ is the probability density matrix for sampling the new photon direction. Eq. (43) shows that $\mathbf{Z}$ depends on four angles $(\theta^{\text{inc}}, \phi^{\text{inc}}, \theta^{\text{sca}}, \phi^{\text{sca}})$, not only on the scattering angle $\Theta$ as does the phase function in the scalar model. Nevertheless we may use $P_{11}$ as PDF for the scattering angle and a random angle between 0 and $2\pi$ for the azimuth direction to sample the scattered direction. The scattered Stokes weight vector is then given by

$$\mathbf{I}_w^{\text{sca}} = P_{11}^{-1}\mathbf{L}(\sigma_2)\mathbf{P}\mathbf{L}(\sigma_1)\mathbf{I}_w^{\text{inc}} = P_{11}^{-1}\mathbf{Z}\mathbf{I}_w^{\text{inc}}, \tag{47}$$

where the weight $P_{11}^{-1}$ corrects for using $P_{11}$ as PDF to sample the scattered direction. This method is also known as importance sampling.

After $n$ scattering events the Stokes weight vector is

$$\mathbf{I}_w^{\mathrm{n}} = \left( \prod_{i=n}^{1} (P_{11}^{-1})_i \mathbf{Z}_i \right) \mathbf{I}_w^0, \tag{48}$$

where i denotes the number of the scattering event. We trace the photon through the atmosphere, either from the sun to the sensor (forward tracing) or from the sensor to the sun (backward tracing) and calculate the product of all scattering matrices. Here it is important that the matrix multiplications are in the correct order as in Eq. (48). The total scattering matrix is then multiplied with the initial Stokes weight vector to get the final Stokes weight vector.

In order to reduce the noise of radiance calculations the local estimate method has also been implemented. A detailed mathematical derivation for scalar radiative transfer is given in (Marshak and Davis, 2005). The method can easily be adapted to polarized radiative transfer.

## 2.2 Rayleigh scattering

Molecular scattering is described by the analytical phase matrix $\mathbf{P}_{\mathrm{R}}$ (Hansen and Travis, 1974)

$$\mathbf{P}_{\mathrm{R}}(\Theta) =$$

$$\Delta \begin{bmatrix} \frac{3}{4}(1+\cos^2\Theta) & -\frac{3}{4}\sin^2\Theta & 0 & 0 \\ -\frac{3}{4}\sin^2\Theta & \frac{3}{4}(1+\cos^2\Theta) & 0 & 0 \\ 0 & 0 & \frac{3}{2}\cos\Theta & 0 \\ 0 & 0 & 0 & \Delta'\frac{3}{2}\cos\Theta \end{bmatrix}$$

$$+(1-\Delta) \begin{bmatrix} 1 & 0 & 0 & 0 \\ 0 & 0 & 0 & 0 \\ 0 & 0 & 0 & 0 \\ 0 & 0 & 0 & 1 \end{bmatrix},$$

where

$$\Delta = \frac{1-\delta}{1+\delta/2}, \qquad \Delta' = \frac{1-2\delta}{1-\delta}, \tag{49}$$

and $\delta$ is the depolarization factor that accounts for the anisotropy of the molecules. The scattering and the absorption coefficients can also be derived analytically.

| Component | rel. humidity (%) | $r_{\mathrm{mod}}$ ($\mu$m) | $r_{\mathrm{min}}$ ($\mu$m) | $r_{max}$ ($\mu$m) | $\sigma$ | $\rho$ (g cm$^{-3}$) | refractive index |
|---|---|---|---|---|---|---|---|
| Water soluble | 95 | 0.0399 | 0.0074 | 42.8 | 2.24 | 1.12 | $1.37 - 7.50 \cdot 10^{-4} i$ |
| Sea salt (acc.) | 95 | 0.605 | 0.0108 | 58.5 | 2.03 | 1.05 | $1.35 - 1.96 \cdot 10^{-8} i$ |
| Soot | 0 | 0.0118 | 0.005 | 20.0 | 2.00 | 1.00 | $1.75 - 4.65 \cdot 10^{-1} i$ |

Table 1: Parameters from the OPAC database (Hess et al., 1998) for 350 nm that were used for Mie calculations to obtain the aerosol scattering phase matrices shown in Fig. 2.

## 2.3 Water cloud scattering

The optical properties of water cloud droplets can be calculated using Mie theory (Mie, 1908), which is for instance implemented in the well known and well validated Mie code by Wiscombe (1980). This code is also part of the *libRadtran* package. For size distribution we assumed a gamma-distribution to generate a database of optical properties:

$$n(r) = Cr^{\alpha} \exp\left(-\frac{(\alpha+3)r}{r_{\mathrm{eff}}}\right) \tag{50}$$

The parameter $\alpha$ was set to 7, a typical value for liquid water clouds. The refractive index of water is another input to the Mie program and the *libRadtran* package includes data published by Warren (1984).

## 2.4 Aerosol scattering

The optical properties of the aerosol database in libRadtran have also been calculated using Mie theory (Mie, 1908). The refractive index of the aerosol particles and the size distributions were taken from the OPAC aerosol database (Hess et al., 1998) for various aerosol types. OPAC also provides typical aerosol type mixtures, for instance for continental polluted or desert conditions. OPAC does not include any information about the aerosol particle shape, so we assume spherical particles although we know that this assumption is not always realistic.

Fig. 2 shows the phase matrices of various OPAC aerosol types, of liquid cloud droplets with an effective radius of 10$\mu$m and, for comparison, the Rayleigh scattering phase matrix. OPAC provides parameters for the log-normal distribution

$$n(r) = \frac{C}{r} \exp\left[-\frac{1}{2}\left(\frac{\ln r - \ln r_{\mathrm{mod}}}{\ln \sigma}\right)^2\right], \tag{51}$$

where $r_{\mathrm{mod}}$ is the mode radius, $\sigma$ measures the width of the distribution, and the constant $C$ is determined by normalisation. Table 1 shows the parameters that were used to compute the phase matrices shown in Fig. 2. OPAC parameters for altogether 10 aerosol types and various relative humidities have been used to produce a dataset of aerosol optical properties including the complete phase matrices so that *libRadtran* allows to define arbitrary mixtures of the basic aerosol types and uses automatically aerosol properties for the relative humidity corresponding to the background atmosphere.

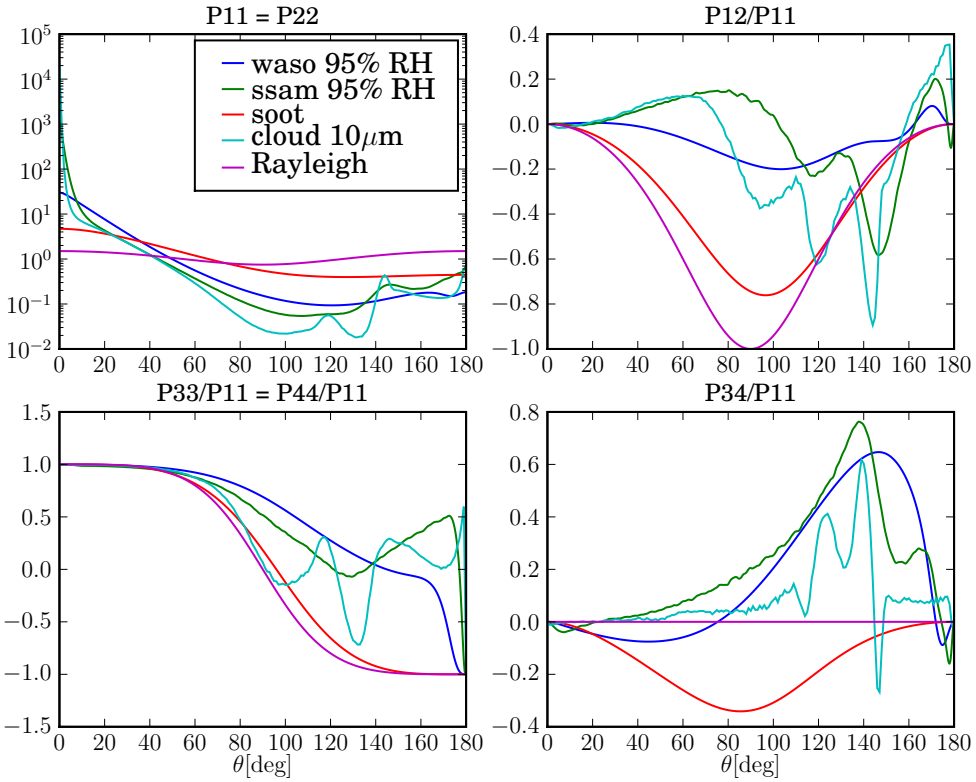


Figure 2: Phase matrix elements for OPAC aerosol types “water soluble” (WASO), “sea salt accumulated mode” (SSAM), and soot, for a liquid water cloud with a droplet effective radius of 10$\mu$m, and for Rayleigh scattering. The wavelength is 350 nm.

Fig. 2 shows that the forward scattering peak increases with particle size. Rayleigh scattering is described by the electromagnetic field of an oscillating dipole with isotropic polarizability (van de Hulst, 1981), therefore the phase matrix element $P_{12}$ for Rayleigh scattering has the minimum at 90°. This means that the linear polarization has its maximum at a scattering angle of 90°. For soot, this minimum is still visible but for other aerosols and for the cloud droplets the angular dependence of $P_{12}$ is completely different which means that we may expect completely different polarization characteristics.

## 2.5 Surface reflection

For polarized radiation, MYSTIC can currently handle Lambertian surfaces and bidirectional polarized reflectance matrices (see section 3.3).

According to Lambert's law the diffusely reflected light is isotropic and is unpolarized, independently of the state of polarization of the incident radiation and the angle of illumination (Chandrasekhar, 1950). This is not valid for real surfaces, especially reflection by water surfaces is strongly polarized.

# 3 Surface bidirectional reflection distribution functions

The surface BRDF (Bidirectional Reflection Distribution Function) describes the distribution of scattered radiance from the surface. Basic reasons for the anisotropy of surface scattering are specular reflectance, rough surfaces, volumetric scattering, and geometric optical surface scattering, see Fig. 3. The surface BRDF and albedo are key parameter for climate simulations and remote sensing applications.

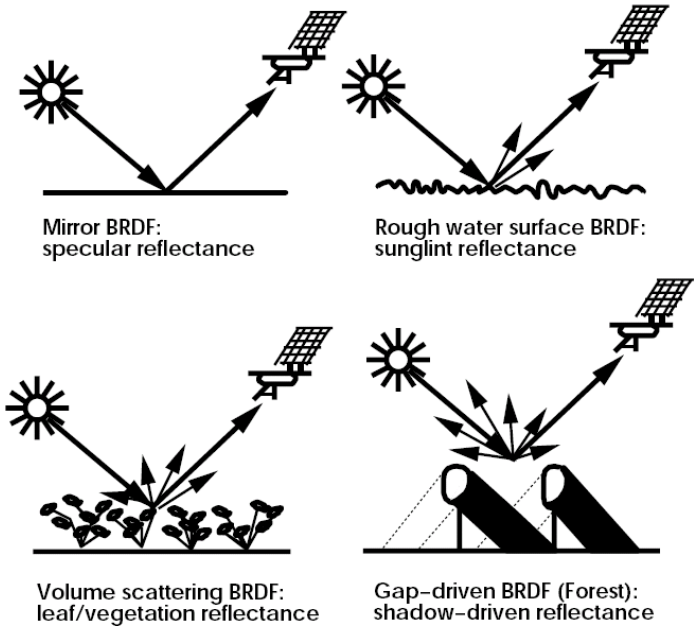


Figure 3: Basic reasons for the anisotropy of surface scattering (from MODIS BRDF/Albedo Product ATBD Version 5).

The BRDF $R$ is defined as the ratio of reflected radiance per unit of incoming irradiance (Marshak and Davis, 2005; Roberts, 2001)

$$R(\theta_i,\Phi_i,\theta_r,\Phi_r,\lambda,P) = \frac{I(\theta_r,\Phi_r)}{\mu_i F_i}. \tag{52}$$

where $(\theta_i,\Phi_i)$ and $(\theta_r,\Phi_r)$ are the directions of the incoming and of the reflected radiance respectively, $F_i$ is the incoming flux, $\mu_i$ is the cosine of the associated zenith angle, and $P$ the wave polarization. The BRDF provides the lower boundary condition for the solution of the radiative transfer Eq. (7).
In order to be physically realistic, the BRDF must fulfill at least the Helmholtz reciprocity principle

$$R(\theta_i,\Phi_i,\theta_r,\Phi_r) = R(\theta_r,\Phi_r,\theta_i,\Phi_i) \tag{53}$$

and energy conservation

$$\int_0^{2\pi} d\Phi_r \int_0^{\pi/2} d\theta_r R(\theta_i,\Phi_i,\theta_r,\Phi_r,\lambda)\sin(\theta_r)\cos(\theta_r) \leq 1. \tag{54}$$

## 3.1 BRDF models

Physically based models are the most complex BRDF models compared to semi-empirical and empirical models. They deal with the underlying physics in an exact way. Physical models aim for describing the geometric shapes of the vegetation (geometric models), treat canopies as a volumes of scattering and absorbing particles (turbid medium models), or even intend to describe them by crowds of individual vegetation elements (complex models).

*Linear Kernel-based* BRDF models have the general form

$$R(\theta_i,\Phi_i,\theta_r,\Phi_r,\lambda) = \sum_k f_k(\lambda) K_k(\theta_i,\theta_r,\Phi), \tag{55}$$

where $K_k$ are the kernels, representing the directional distribution of the scattered light, $f_k$ are spectrally dependent parameters derived from measurements, and $\Phi = \Phi_i - \Phi_r$ is the relative azimuth of the reflection event. Following Roujean et al. (1992) most of the recent models use a three Kernel structure:

$$R(\theta_i,\Phi_i,\theta_r,\Phi_r,\lambda) = f_{iso}(\lambda) + f_{vol}(\lambda) K_{vol}(\theta_i,\theta_r,\Phi) + f_{geo}(\lambda) K_{geo}(\theta_i,\theta_r,\Phi). \tag{56}$$

The *Ross-Thick* volume scattering kernel $K_{vol}$ is commonly defined as follows:

$$K_{vol}(\theta_i,\theta_r,\Phi) = \frac{4}{3\pi}\frac{1}{\cos(\theta_i)+\cos(\theta_r)}\left[\left(\frac{\pi}{2}-\zeta\right)\cos\zeta + \sin\zeta\right] - \frac{1}{3}, \tag{57}$$

where $\zeta$ is the phase angle of scattering defined as

$$\zeta = \cos^{-1}(\cos\theta_i\cos\theta_r + \sin\theta_i\sin\theta_r\cos\Phi). \tag{58}$$

The description of the *geometric-optical* kernel $K_{geo}$ is still under discussion. The *Roujean* model (Roujean et al., 1992) uses the following expression

$$\begin{aligned} K_{geo}(\theta_i,\theta_r,\Phi) &= \frac{1}{2\pi}[(\pi-\Phi)\cos\Phi + \sin\Phi]\tan\theta_i\tan\theta_r \\ &\quad -\frac{1}{\pi}\left[\tan\theta_i + \tan\theta_r + \sqrt{\tan^2\theta_i + \tan^2\theta_r + 2\tan\theta_i\tan\theta_r\cos\Phi}\right]. \end{aligned} \tag{59}$$

The *non-reciprocal Li-Sparse (LS)* model (Li and Strahler, 1992; Li et al., 1996) is designed for simulation of sparse vegetation covers like grass, shrub lands, emerging crops or bare soil surfaces. It uses the following geometric kernel:

$$K_{geo}(\theta_i,\theta_r,\Phi) = \frac{1}{\pi}(t-\sin t\cos t)(\sec\theta_i+\sec\theta_r) - (\sec\theta_i+\sec\theta_r) + \frac{1}{2}(1+\cos\zeta)\sec\theta_r, \tag{60}$$

where

$$\cos t = \frac{\sqrt{D^2 + (\tan\theta_i\tan\theta_r\cos\Phi)^2}}{(\sec\theta_i+\sec\theta_r)} \tag{61}$$

and

$$D = \sqrt{\tan^2\theta_i + \tan^2\theta_r - 2\tan\theta_i \tan\theta_r \cos\Phi}. \tag{62}$$

The *reciprocal Li-Sparse (LSR)* model is a slightly modified version of the LS model which satisfies the Helmholtz reciprocity Eq. (53)

$$K_{geo}(\theta_i,\theta_r,\Phi) = \frac{1}{\pi}(t - \sin t\cos t)(\sec\theta_i + \sec\theta_r) - (\sec\theta_i + \sec\theta_r) + \frac{1}{2}(1+\cos\zeta)\sec\theta_i \sec\theta_r. \tag{63}$$

The *Li-Dense* model is primarily designed for simulating dense canopies of high reaching vegetation covers. It uses the following geometric kernel:

$$K_{geo}(\theta_i,\theta_r,\Phi) = \frac{1+\cos\zeta\sec\theta_r}{\cos\theta_i + \cos\theta_r - (t-\sin t\cos t)(\sec\theta_i+\sec\theta_r)/\pi} - 2. \tag{64}$$

The *RPV* model (Rahman et al., 1993) is a semi-empirical multiplicative BRDF model. It is able to describe the BRDF of arbitrary natural surfaces, ranging from bare soil to canopy covers. The model expresses surface anisotropy using three terms: $\rho_0$ characterizes the intensity of the reflectance, $k$ describes the surface anisotropy and $\Theta$ controls the relative amount of forward and backward scattering.

$$R(\theta_i,\Phi_i,\theta_r,\Phi_r,\lambda) = \rho_0 \frac{\cos^{k-1}\theta_i \cos^{k-1}\theta_r}{(\cos\theta_i+\cos\theta_r)^{1-k}} F(g)[1+R(G)], \tag{65}$$

where $F(g)$ describes the ratio between forward and backward scattering

$$F(g) = \frac{1-\Theta^2}{[1+\Theta^2 - 2\Theta\cos(\pi-g)]^{1.5}}. \tag{66}$$

The phase angle $g$ is given by

$$\cos g = \cos\theta_i\cos\theta_r + \sin\theta_i \sin\theta_r \cos(\Phi_i - \Phi_r). \tag{67}$$

The hot spot effect is expressed by

$$1 + R(G) = 1 + \frac{1-\rho_0}{1+G}. \tag{68}$$

and the geometric factor $G$ is given by

$$G = [\tan^2\theta_i + \tan^2\theta_r - 2\tan\theta_i \tan\theta_r \cos(\Phi_i - \Phi_r)]^{1/2}. \tag{69}$$

## 3.2 The AMBRALS BRDF Modeling Framework

The AMBRALS (Algorithm for Modeling [MODIS] Bidirectional Reflectance Anisotropies of the Land Surface) by Wanner et al. (1997) allows a variety of kernel-driven semi-empirical BRDF models to be explored. It has been developed for the production of the MODIS BRDF/albedo product. Both the RossThick and LiSparse-R kernels are among the large number of kernels available and therefore the RossThick/LiSparse-R BRDF model used in the MODIS product can be specified and used. The kernels are based on the theory by Roujean et al. (1992) described above and on Cox and Munk (1954). The parameters for describing the AMBRALS BRDF are available from `http://www-modis.bu.edu/brdf/product.html` on a 1km spatial resolution.

## 3.3 Bidirectional polarized reflectance function (BPDF) for the ocean surface

Polarization by surface reflection has been included into MYSTIC so that arbitrary reflectance matrices can be handled.

A program by Mishchenko and Travis (1997) freely available at `http://www.giss.nasa.gov/staff/mmishchenko/brf/` has been implemented into *libRadtran* to compute the reflectance matrix for rough water surfaces. The model is based on the Fresnel equations, on Cox and Munk (1954) to describe the wind-speed dependent slope of the waves, and on Tsang et al. (1985) to account for shadowing effects.

For directions of light incidence and reflection $\mathbf{n}_0 = (-\mu_0, \phi_0)$ and $\mathbf{n} = (-\mu, \phi)$, respectively, the ocean reflectance matrix is

$$\mathbf{R}_0(\mu, \mu_0, \phi - \phi_0) = \frac{|\mathbf{k}_d|^4}{4\mu\mu_0 \, |\mathbf{n} \times \mathbf{n}_0|^4 \, k_{dz}^4 2s^2} \exp\left(-\frac{k_{dx}^2 + k_{dy}^2}{2k_{dz}^2 s^2}\right) \mathbf{M}(\mu, \mu_0, \phi - \phi_0), \tag{70}$$

where

$$\mathbf{k}_d = k\,(\mathbf{n} - \mathbf{n}_0) = k_{dx}x + k_{dy}y + k_{dz}z. \tag{71}$$

$s^2$ is the mean surface slope of the waves which is related to the wind speed by the empirically derived equation (Cox and Munk, 1954):

$$2s^2 = 0.003 + 0.00512W \tag{72}$$

where $W$ is the near-surface wind speed in meters per second. The exponential term in Eq. 70 describes the distribution of the surfaces slopes that is assumed to be Gaussian. $k = 2\pi/\lambda$ is the free-space wavenumber for the wavelength $\lambda$.

The elements of the $4\times4$ matrix $\mathbf{M}$ can be derived from the Fresnel equations and geometrical considerations and are given in the appendix of Mishchenko and Travis (1997). The Fresnel equations describe the behaviour of light when moving between media with different complex

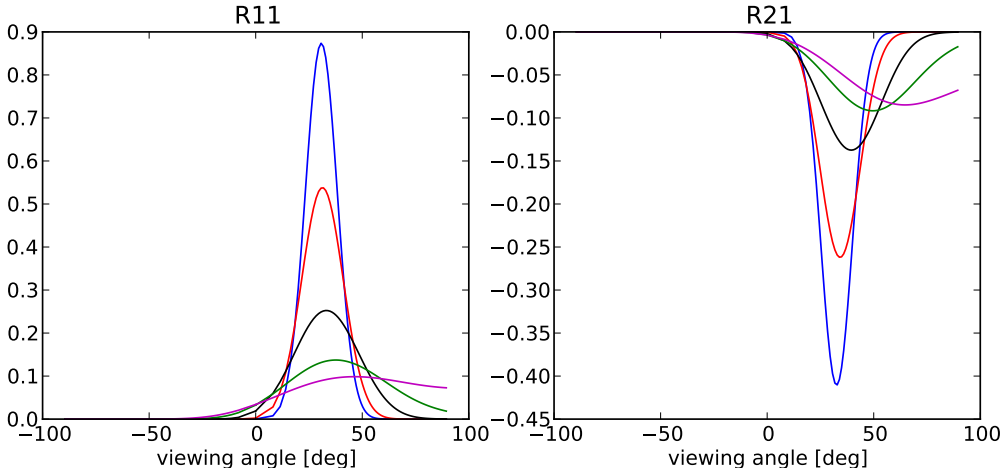


Figure 4: Two elements of the normalized polarized reflectance matrix by Mishchenko and Travis (1997). The sun position is at -30°. R11 corresponds to the BRDF. The element R12 can be related to the polarization in the principle plane.

refractive indices $m_1$ and $m_2$, i.e. the reflection and refraction of the light. The fraction of the incident power that is reflected from the interface is given by the reflectance $R$ and the fraction that is refracted is given by the transmittance $T$. The reflected light that is polarized perpendicular to the reference plane is given by

$$R_r = \frac{m_1 \cos\alpha - m_2 \cos\beta}{m_1 \cos\alpha + m_2 \cos\beta} \tag{73}$$

where $\alpha$ is the incident angle with respect to the surface normal and $\beta$ is the angle of the refracted beam to the surface normal. The parallel polarized component is given by

$$R_l = \frac{m_2 \cos\alpha - m_1 \cos\beta}{m_2 \cos\alpha + m_1 \cos\beta} \tag{74}$$

To take the effects of shadowing by surface waves into account the ocean reflection matrix is multiplied by a bidirectional shadowing function $S(\mu,\mu_0)$ defined by Tsang et al. (1985):

$$S(\mu,\mu_0) = \frac{1}{1+\Lambda(\mu)+\Lambda(\mu_0)}, \tag{75}$$

where

$$\Lambda(\mu) = \frac{1}{2}\left[\left(\frac{2(1-\mu^2)}{\pi}\right)^{1/2}\frac{s}{\mu}\exp\left(-\frac{\mu^2}{2s^2(1-\mu^2)}\right) - \mathrm{erfc}\left(\frac{\mu}{s\sqrt{2(1-\mu^2)}}\right)\right]. \tag{76}$$

erfc(x) is the complementary error function. Fig. 4 shows two elements of the ocean reflectance matrix.

The implementation of the reflectance matrix in MYSTIC is as follows: Each time a photon hits the surface the probability for being reflected into the direction towards the sensor is calculated

using the reflection matrix. In order to do this the Stokes weight vector $\mathbf{I}_0$ is multiplied with the reflectance matrix obtained for the incident direction and the direction towards the sensor. The total Stokes weight vector for a photon path with one surface reflection after $m$ scatterings can be written as (compare section 2):

$$\mathbf{I}_w^{\mathrm{n}} = \left( \prod_{i=n}^{m+1} (P_{11}^{-1})_i \mathbf{Z}_i \right) \mathbf{R} \left( \prod_{i=m}^{1} (P_{11}^{-1})_i \mathbf{Z}_i \right) \mathbf{I}_w^0, \tag{77}$$

The sum of the Stokes weight vectors of all photons equals the radiance for the viewing direction of the sensor.

# References

Chance, K. and Spurr, R. J. D.: Ring effect studies: Rayleigh scattering including molecular parameters for rotational Raman scattering, and the Fraunhofer spectrum, Appl. Opt., 36, 5224–5230, 1997.

Chandrasekhar, S.: Radiative transfer, Oxford Univ. Press, UK, 1950.

Cox, C. and Munk, W.: Measurement of the roughness of the sea surface from photographs of the sun's glitter, Journal of the Optical Society of America, 44, 838–850, 1954.

Dahlback, A. and Stamnes, K.: A new spherical model for computing the radiation field available for photolysis and heating at twilight, Planet. Space Sci., 39, 671–683, 1991.

de Haan, J. F., Veefkind, J. P., van Oss, R., Levelt, P. F., and Noordhoek, R.: Accounting for Raman scattering in DOAS, Tech. rep., SN-OMIE-KNMI-409, 2003.

Emde, C. and Mayer, B.: Simulation of solar radiation during a total solar eclipse: A challenge for radiative transfer, Atmos. Chem. Phys., 7, 2259–2270, 2007.

Emde, C., Buras, R., Mayer, B., and Blumthaler, M.: The impact of aerosols on polarized sky radiance: model development, validation, and applications, Atmospheric Chemistry and Physics Discussions, 9, 17 753–17 791, http://www.atmos-chem-phys-discuss.net/9/17753/2009/, 2009.

Hansen, J. E. and Travis, L. D.: Light scattering in planetary atmospheres, Space Science Reviews, 16, 527–610, 1974.

Hess, M., Koepke, P., and Schult, I.: Optical Properties of Aerosols and Clouds: The Software Package OPAC, Bulletin of the American Meteorological Society, 79, 831–844, 1998.

Jackson, J. D.: Classical Electrodynamics, John Wiley & Sons, New York, 1975.

Kattawar, G. W., Young, A. T., and Humphreys, T. J.: Inelastic scattering in planetary atmospheres. I. The Ring effect, without aerosols, The Astrophysical Journal, 243, 1049–1057, 1981.

Kylling, A. and Stamnes, K.: Efficient yet accurate solution of the linear transport equation in the presence of internal sources: the exponential–linear–in–depth approximation, J. Com. Phys., 102, 265–276, 1992.

Landgraf, J., Hasekamp, O. P., van Deelen, R., and Aben, I.: Rotational Raman scattering of polarized light in the Earth atmosphere: a vector radiative transfer model using the radiative transfer perturbation theory approach, J. Quant. Spectrosc. Radiat. Transfer, 87, 399–433, 2004.

Li, X. and Strahler, A. H.: Geometric-optical bi-directional reflectance modeling of the discrete crown vegetation canopy: effect of crown shape and mutual shadowing, IEEE Transactions on Geoscience and Remote Sensing, 30, 276–292, 1992.

Li, Z., Cihlar, J., Zheng, X., Morceau, L., and Ly, H.: The bidirectional effects of AVHRR measurements over Boreal regions, IEEE Transactions on Geoscience and Remote Sensing, 34, 1308–1322, 1996.

Marshak, A. and Davis, A.: 3D Radiative Transfer in Cloudy Atmospheres, Springer, iSBN-13 978-3-540-23958-1, 2005.

Mayer, B.: I3RC phase 1/2 results from the MYSTIC Monte Carlo model, in: Intercomparison of three-dimensional radiation codes: Abstracts of the first and second international workshops, edited by Cahalan, R. and Davis, R., pp. 49–54/107–108, Institute of Atmospheric Physics, University of Arizona, iSBN 0-9709609-0-5, 2000.

Mayer, B. and Kylling, A.: Technical note: the libRadtran software package for radiative transfer calculations-description and examples of use, Atmos. Chem. Phys., 5, 1855–1877, 2005.

Mie, G.: Beiträge zur Optik trüber Medien, speziell kolloidaler Metallösungen, Annalen der Physik, 330, 377–445, doi:10.1002/andp.19083300302, 1908.

Mishchenko, M. I. and Travis, L. D.: Satellite retrieval of aerosol properties over the ocean using polarization as well as intensity of reflected sunlight, J. Geophys. Res., 102, 16 989–17 013, 1997.

Mishchenko, M. I., Travis, L., and Lacis, A.: Scattering, Absorption, and Emission of Light by Small Particles, Cambridge University Press, 2002.

Rahman, H., Pinty, B., and Verstraete, M. M.: Coupled surface–atmosphere reflectance (CSAR) model 2. semiempirical surface model usable with NOAA advanced very high resolution radiometer data, J. Geophys. Res., 98, 20,791–20,801, 1993.

Roberts, G.: A review of the application of BRDF models to infer land cover parameters at regional and global scales, Progress in Physical Geography, 25, 483–511, 2001.

Roujean, J.-L., Leroy, M., and Deschamps, P.: A bidirectional reflectance model of the Earth's surface for the correction of remote sensing data, J. Geophys. Res., 97, 20 455–20 468, 1992.

Spurr, R., de Haan, J. D., van Oss, R., and Vasilkov, A.: Discrete ordinate radiative transfer in a stratified medium with first order rotational Raman scattering, J. Quant. Spectrosc. Radiat. Transfer, 109, 404–425, 2008.

Stamnes, K.: The Theory of Multiple Scattering of Radiation in Plane Parallel Atmospheres, Reviews of Geophysics, 24, 299–310, 1986.

Stamnes, K., Tsay, S.-C., Wiscombe, W., and Jayaweera, K.: Numerically stable algorithm for discrete–ordinate–method radiative transfer in multiple scattering and emitting layered media, Appl. Opt., 27, 2502–2509, 1988.

Stamnes, K., Tsay, S.-C., Wiscombe, W., and Laszlo, I.: DISORT, a General-Purpose Fortran Program for Discrete-Ordinate-Method Radiative Transfer in Scattering and Emitting Layered Media: Documentation of Methodology, Tech. rep., Dept. of Physics and Engineering Physics, Stevens Institute of Technology, Hoboken, NJ 07030, 2000.

Tsang, L., Kong, J. A., and Shin, R. T.: Theory of Microwave Remote Sensing, John Wiley, New York, 1985.

van de Hulst, H. C.: Light Scattering by Small Particles, Dover, 1981.

Vountas, M., Rozanov, V. V., and Burrows, J. P.: Ring effect: impact of rotational Raman scattering on radiative transfer in Earth's atmosphere, J. Quant. Spectrosc. Radiat. Transfer, 60, 943–961, 1998.

Wanner, W., Strahler, A. H., Hu, B., Lewis, P., Muller, J.-P., Li, X., Schaaf, C. L. B., and Barnsley, M. J.: Global retrieval of bidirectional reflectance and albedo over land from EOS MODIS and MISR data: Theory and algorithm, J. Geophys. Res., 102, 17 143–17 161, 1997.

Warren, S. G.: Optical constants of ice from the ultraviolett to the microwave, Applied Optics, 23, 1206–1225, 1984.

Wiscombe, W.: Improved Mie scattering algorithms, Applied Optics, 19, 1505–1509, 1980.

Young, A. T.: On the Rayleigh–scattering optical depth of the atmosphere, J. of Applied Meteorology, 20, 328–330, 1981a.

Young, A. T.: Rayleigh scattering, Appl. Opt, 20, 533–535, 1981b.